Lithographic characterization of the field dependent astigmatism and alignment stability of a 0.3 numerical aperture extreme ultraviolet microfield optic

Patrick P. Naulleau[a)]
College of Nanoscale Science and Engineering, University at Albany, New York 12203

Jason P. Cain
EECS Department, University of California, Berkeley, California 94720

Kenneth A. Goldberg
Center for X-Ray Optics, Lawrence Berkeley National Laboratory, Berkeley, California 94720

(Received 10 May 2005; accepted 18 July 2005; published 14 September 2005)

Here we describe the lithographic characterization of the astigmatism in a 0.3-numerical aperture extreme ultraviolet (EUV) microexposure tool installed at Lawrence Berkeley National Laboratory. The lithographic results, measured across the field of view, are directly compared to EUV interferometry results obtained from the same tool at Berkeley during the optic alignment phase nearly one year prior to the lithographic characterization. The results suggest a possible long-term astigmatism drift on the order of 0.5 nm rms. Moreover, the uncertainty in the lithographic characterization is shown to be approximately 0.1 nm rms, similar to the precision previously demonstrated from EUV interferometry. © *2005 American Vacuum Society.*
[DOI: 10.1116/1.2037647]

I. INTRODUCTION

Extreme ultraviolet (EUV) lithography[1] is a leading candidate for high-volume manufacturing of nanoelectronic devices at feature sizes of 32 nm and below. To enable the development of supporting technologies, such as resists and masks, 32 nm capable microfield EUV lithography tools have recently been developed. One such tool has been operational at Lawrence Berkeley National Laboratory since early 2004.[2,3] The Berkeley tool utilizes a synchrotron as its source of EUV radiation along with a programmable coherence illuminator[4] that enables the nominally coherent synchrotron source[5,6] to be used for lithography. The lithographic optic used in the Berkeley tool is a 0.3 numerical aperture (NA) Micro-Exposure Tool (MET) optic.[7,8] The MET optic is a centrally obscured, two element, axially symmetric 5×-reduction optical system manufactured by Zeiss. The central obscuration has a radius equal to 30% of the full pupil radius, producing an annular clear aperture.

Operating at a wavelength of 13.5 nm and utilizing reflection optics, EUV lithography systems require extremely tight alignment tolerances. This makes optical housing stability crucial for reliable EUV performance. Optical system alignment errors manifest themselves primarily as low-order aberrations such as first-order astigmatism, coma, and spherical error. This is especially true for smaller scale systems like the MET optic, which is comprised of only two optical elements. Here we describe the lithographic characterization of the field-dependent astigmatism error in the Berkeley tool. The lithographic results are directly compared to EUV interferometry results obtained from the same tool at Berkeley during the optic alignment phase nearly one year prior to the lithographic characterization. The results suggest a possible long-term astigmatism drift on the order of 0.5 nm rms. Moreover, the uncertainty in the lithographic characterization is shown to be approximately 0.1 nm rms.

II. MEASUREMENT METHOD

Numerous methods exist for print-based quantitative aberration extraction,[9–11] however, these methods typically rely on the use of phase shift masks and/or the ability to print at the diffraction limit of the optic. Both these restrictions are problematic given the current status of EUV lithography. Phase shift EUV masks are difficult to fabricate at any resolution let alone the diffraction-limited resolution required for aberration characterization. Moreover, current resist technology is limited to resolving at approximately twice the diffraction limit of 0.3 NA EUV optics. These limitations preclude using the methods described in the literature for EUV applications at the present time.

Given that the immediate goal of the work presented here is to characterize the alignment stability of the MET optic, we can safely restrict ourselves to measuring only a small subset of the possible aberrations. Perhaps the simplest aberration to measure using conventional printing is astigmatism. Astigmatism can be viewed as a longitudinal focus shift between features in different orientations. To fully characterize the astigmatism (magnitude and direction), we need to measure the relative longitudinal focal position for four different feature orientations, for example, 0°, 90°, 45°, and −45°. Although using finer resolution patterns can be helpful for improving the sensitivity to focus, there is no requirement to print features at or even near the diffraction limit.

[a)]Author to whom correspondence should be addressed; electronic mail: pnaulleau@uamail.albany.edu

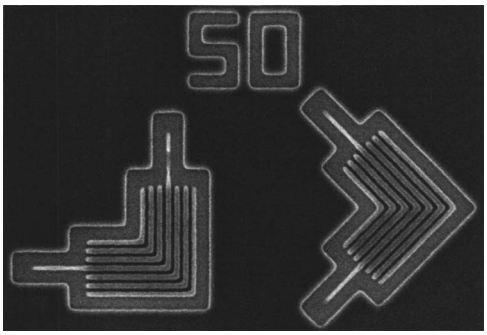

FIG. 1. Scanning electron microscope (SEM) image of the printed elbow features used to extract the astigmatism data. The 0° and 45°-oriented elbow patterns are placed in close proximity to each other on the mask such that focus and dose can safely be assumed to be constant over all the orientations of interest.

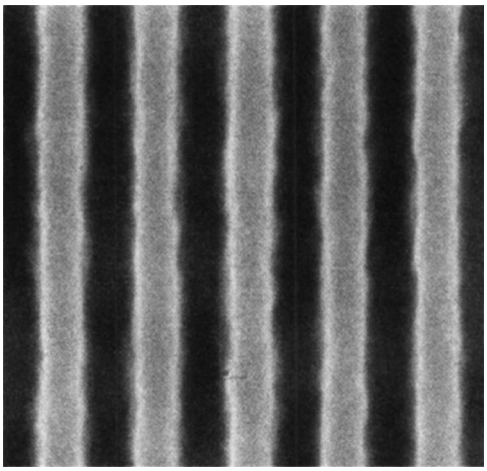

FIG. 2. Representative SEM image used in the focus analysis for 0°-oriented features. Each feature orientation is imaged separately at a magnification of 200 000. In all cases, the SEM image acquisition is rotated such that the features appear vertical in the captured image.

Longitudinal focus position is experimentally determined by printing a focus-exposure matrix with focus steps of 50 nm or smaller. The through-focus imagery is then analyzed to determine the best focus as a function of feature orientation. The analysis is based on quadratic polynomial regression to the through-focus printed linewidth, or critical dimension (CD). The exposure dose used for the analysis is chosen to be safely away from the iso-focal point. Best focus is chosen to correspond to the minimum point of the quadratic fit. Alternatively, through-focus line-edge roughness (LER) data could be used to find optimal focus. We note also that the entire process-window data could be collected to perhaps further refine the focus measurement. From the focus offset between 0° and 90°-oriented features we can determine the 0° astigmatism. The 45° astigmatism is determined from focus offset between the 45° and −45° features. Focus offset is linearly related to astigmatism magnitude. For the MET optic of interest here, aerial-image modeling[12] has been used to determine a scaling ratio of 55 nm relative orthogonal-feature focus shift per 0.5 nm rms astigmatism as measured on the annular pupil.

Figure 1 shows a scanning electron microscope (SEM) image of the printed 50 nm elbow features used to extract the astigmatism data. The 0° and 45°-oriented elbow patterns are placed in close proximity to each other on the mask such that focus and dose can safely be assumed to be constant over all the orientations of interest. To measure the astigmatism across the field, this same feature set is replicated at nine points across the 200×600 μm field in a 3×3 grid, nominally matching the field points measured during interferometric alignment of the optic.[13] The SEM imagery actually used for determination of focus is taken at a magnification of 200 000× and each feature orientation is imaged separately. Figure 2 shows a representative SEM image of the 0°-oriented component of the 50 nm elbow pattern. In all cases, the SEM image acquisition is rotated such that the features appear as vertical in the captured image.

III. MEASUREMENT RESULTS

The measurement method described above has been used to lithographically characterize the astigmatism in the MET optic at Berkeley. A focus step size of 40 nm was used, and 50 nm patterns, as shown in Figs. 1 and 2, were analyzed. The patterns were recorded in a 125-nm-thick layer of Rohm and Haas *MET-1K* resist (XP3454C). Postapplication and exposure bake temperatures were 120 °C and the bake times were 60 and 90 s, respectively. The lithographic measurement was performed nearly one year after completion of the interferometric alignment of the optical system.[13] In addition to the long time delay, reconfiguration of the interferometer into an exposure tool[14] involved some handling of the optic. Interferometric measurements have shown the MET optic to be sensitive to operational temperature, thus care is taken to ensure that the lithography in general and these measurements in particular are performed at the same temperature as used during interferometric alignment. Figure 3 shows the measured astigmatism across the field in a 3×3 grid. Both the individual astigmatism components as well as the total

0° astigmatism

-0.467	-0.434	-0.188
-0.518	-0.427	-0.036
-0.481	-0.511	-0.002

45° astigmatism

-0.003	-0.237	-0.314
-0.032	-0.079	-0.216
-0.032	-0.089	-0.160

Total astigmatism magnitude

0.468	0.494	0.365
0.519	0.433	0.219
0.482	0.518	0.160

FIG. 3. Astigmatism measured lithographically at nine points in a 3×3 grid spanning the field of view. The reported results are rms magnitudes in nanometers. The locations in the table correspond to the relative physical locations of the measured points in the field.

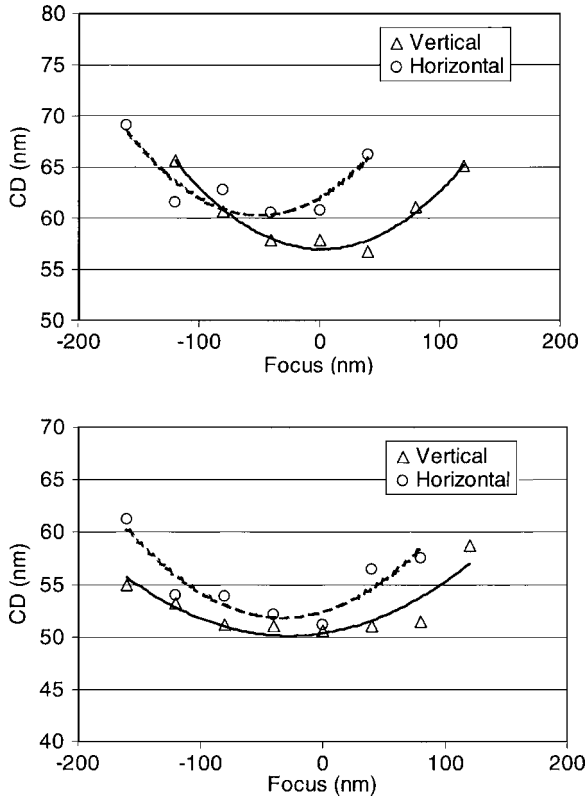

FIG. 4. Through-focus CD data and quadratic fits for two representative field points from the measured 3×3 grid of field points. (a) Corresponds to the row 1, column 1 point and (b) to the row 2, column 3 point. The horizontal and vertical feature data, corresponding to the 0° astigmatism, is shown.

astigmatism magnitudes are shown. The locations in the table correspond to the relative physical locations of the measured points in the printed field.

Figure 4 shows through-focus CD data for two representative locations in the field, the rms uncertainty in each CD measurement is approximately 0.7 nm. The horizontal and vertical feature data, corresponding to the 0° astigmatism is shown. Figure 3(a) corresponds to the 0° astigmatism value in row 1, column 1 (−0.467 nm), and Fig. 3(b) corresponds to the row 2, column 3 value (−0.036 nm). The CD plots also reveal a horizontal to vertical bias, with the horizontal features printing larger than the vertical features. This is presumably due to the mask shadowing[15] induced by the three-dimensional structure of the mask combined with the off-axis illumination (4° from normal in the *y*-*z* plane, where vertical lines are defined to run in the *y* direction).

To determine the uncertainty in the measured longitudinal focus position (and thus astigmatism) values, a focus test wafer was exposed. This wafer was similar to the astigmatism test wafer, but a single dose was used and the focus step size was 50 nm. Thus instead of a focus exposure matrix, we now have a series of nominally identical through-focus columns in the matrix that we can use to determine the precision of the focus measurement. Based on a total of ten through-focus columns, we find the $1-\sigma$ focus-measurement uncertainty to be 8.8 nm. Assuming this error to be uncorrelated as a function of feature orientation, the focus-offset uncertainty

0° astigmatism

-0.239	0.001	0.317
-0.355	-0.073	0.379
-0.275	-0.065	0.688

45° astigmatism

0.157	-0.035	-0.356
-0.173	-0.013	-0.160
-0.030	-0.031	0.211

Total astigmatism magnitude

0.286	0.035	0.476
0.394	0.074	0.412
0.277	0.072	0.719

FIG. 5. Astigmatism measured interferometrically at nine points in a 3×3 grid spanning the field of view. The reported results are rms magnitudes in nanometers. The locations in the table correspond to the relative physical locations of the measured points in the field.

is 12.5 nm. Based on the focus shift to astigmatism magnitude scaling stated above, this focus error corresponds to a 0.1 nm rms astigmatism uncertainty.

The precision of the lithographic measurement was further evaluated by repeating the astigmatism measurement on a second wafer over a subset of the field. A total of four field points were analyzed in this comparison, yielding eight measurements taking into consideration the two individual astigmatism components. The root mean square error between the two data sets was 0.069 nm on the individual astigmatism components, with the maximum and minimum differences being 0.128 and 0.009 nm, respectively. The root mean square error on the measured total astigmatism magnitude was 0.064 nm. These direct reproducibility results are somewhat better than the uncertainty predicted from the focus repeatability test wafer described above. If this observed difference is statistically meaningful, it could arise from the fact that the focus test wafer used a different focus step size (50 nm vs 40 nm), or that the focus measurement errors are not completely uncorrelated as a function of feature orientation. In fact, it is evident that errors arising from physical focus or dose control problems in the tool would be correlated as a function of orientation. Also, the fact that the measured precision on the total astigmatism magnitude was no worse than that of the individual components also indicates that the relevant errors are not completely uncorrelated as a function of orientation. We note that the two compared astigmatism-measurement wafers were exposed one month apart, thus, the stability of the optic over this time frame is at least as good as the above claimed precision.

Finally, we compare the lithographic results to interferometric results obtained nearly a year earlier. Figure 5 shows the cross-field interferometrically measured astigmatism data and Fig. 6 shows the difference between the interferometric and lithographic results. We see significant discrepancies both in the total astigmatism magnitude and the individual astigmatism components. Errors near 0.5 nm are evident

0° astigmatism

-0.228	-0.436	-0.504
-0.163	-0.354	-0.415
-0.206	-0.445	-0.690

45° astigmatism

-0.161	-0.202	0.041
0.141	-0.065	-0.056
-0.001	-0.059	-0.371

Total astigmatism magnitude

0.182	0.459	-0.111
0.125	0.359	-0.193
0.205	0.446	-0.559

FIG. 6. Difference between interferometric and lithographic measurements of the astigmatism at nine points in a 3×3 grid spanning the field of view. The reported results are rms magnitudes in nanometers. The locations in the table correspond to the relative physical locations of the measured points in the field. The total astigmatism magnitude error is the difference in the total magnitudes of the two measurements and not the total magnitude of the error (defined as the quadratic addition of the individual errors). Negative values of total astigmatism magnitude indicate that the lithographic measurement yielded a smaller value of astigmatism.

over a large portion of the field. The total astigmatism magnitude error shown in Fig. 6 is the difference in the total magnitudes of the two measurements and not the total magnitude of the error (defined as the quadratic addition of the individual errors). Negative values of total astigmatism magnitude indicate that the lithographic measurement yielded a smaller value of astigmatism, thus, at some points in the field the astigmatism has actually improved over time.

IV. DISCUSSION

The field-dependent astigmatism in the 0.3 NA MET optic has been measured lithographically using an orientation-dependent focus-shift method. Reproducibility measurements have demonstrated the uncertainty in the lithographic astigmatism values to be approximately 0.1 nm rms. This compares favorably with the 0.06 nm precision previously demonstrated from EUV interferometry.[13] Comparisons between interferometric measurements and lithographic measurements performed nearly one year later indicate that alignment drifts have occurred affecting the astigmatism by nearly 0.5 nm rms over much of the field. Despite this large change, the field-averaged astigmatism is not greatly increased from the interferometric state: 0.31 nm for the interferometry measurement versus 0.41 for the lithographic measurement. We believe the astigmatism changes to be the results of an alignment drift in the optic, however, one cannot definitely rule out accuracy errors in the interferometric data. Although the precision of the interferometric astigmatism measurement has been shown to be approximately 0.06 nm, accuracy is much more difficult to gauge.

ACKNOWLEDGMENTS

The authors are greatly indebted to Paul Denham and Brian Hoef for expert support with the exposure tool. The authors would also like to thank Robert Brainard and Thomas Koehler of Rohm and Haas for resist and process support and Kim Dean of SEMATECH for programmatic support. This research was performed at Lawrence Berkeley National Laboratory and supported by SEMATECH. Lawrence Berkeley National Laboratory is operated under the auspices of the Director, Office of Science, Office of Basic Energy Sicence, of the U.S. Department of Energy.

[1] R. Stulen and D. Sweeney, IEEE J. Quantum Electron. **35**, 694 (1999).
[2] P. Naulleau, K. Goldberg, J. Cain, E. Anderson, P. Denham, K. Jackson, S. Rekawa, F. Salmassi, and G. Zhang, J. Vac. Sci. Technol. B **22**, 2962 (2004).
[3] P. Naulleau, K. Goldberg, E. Anderson, J. Cain, P. Denham, B. Hoef, K. Jackson, A. Morlens, S. Rekawa, and K. Dean, Proc. SPIE 5751 (to be published).
[4] P. Naulleau, P. Denham, B. Hoef, and S. Rekawa, Opt. Commun. **234**, 53 (2004).
[5] D. Attwood, G. Sommargren, R. Beguiristain, K. Nguyen, J. Bokor, N. Ceglio, K. Jackson, M. Koike, and J. Underwood, Appl. Opt. **32**, 7022 (1993).
[6] C. Chang, P. Naulleau, E. Anderson, and D. Attwood, Opt. Commun. **182**, 24 (2000).
[7] J. Taylor, D. Sweeney, R. Hudyma, L. Hale, T. Decker, G. Kubiak, W. Sweatt, and N. Wester, 2nd International EUVL Workshop, San Francisco, CA, 19–20 October 2000 (proceedings available from SEMA TECH, Austin, TX 78741, www.sematech.org).
[8] R. Hudyma, J. Taylor, D. Sweeney, L. Hale, W. Sweatt, and N. Wester, 2nd International EUVL Workshop, San Francisco, CA, 19–20 October 2000 (proceedings available from SEMATECH, Austin, TX 78741, www.sematech.org
[9] P. Dirksen, C. Juffermans, R. Pellens, M. Maenhoudt, and P. Debisschop, Proc. SPIE **3679**, 77 (1999).
[10] H. Fukuda, K. Hayano, and S. Shirai, J. Vac. Sci. Technol. B **17**, 3318 (1999).
[11] G. Robins, K. Adam, and A. Neureuther, J. Vac. Sci. Technol. B **20**, 338 (2002).
[12] Aerial image modeling was performed using the PROLITH modeling package from KLA-Tencor, San Jose, CA 95134.
[13] K. Goldberg, P. Naulleau, P. Denham, S. Rekawa, K. Jackson, E. Anderson, and J. Liddle, J. Vac. Sci. Technol. B **22**, 2956 (2004).
[14] P. Naulleau, K. Goldberg, E. Anderson, K. Bradley, R. Delano, P. Denham, R. Gunion, B. Harteneck, B. Hoef, H. Huang, K. Jackson, M. Jones, D. Kemp, J. Liddle, R. Oort, A. Rawlins, S. Rekawa, F. Salmassi, R. Tackaberry, C. Chung, L. Hale, D. Phillion, G. Sommargren, and H. Taylor, Proc. SPIE **5374**, 881 (2004).
[15] B. Bollepalli, M. Khan, and F. Cerrina, J. Vac. Sci. Technol. B **16**, 3444 (1998).